Journal of the European Ceramic Society **14** (1994) 153–161

R-Curve Behaviour in Ceramic Composites Produced by Directed Metal Oxidation

J. Rödel,[a,*] M. Sindel,[a] M. Dransmann,[b] R. W. Steinbrech[b] & N. Claussen[a]

[a] Advanced Ceramics Group, Technische Universität Hamburg–Harburg, Germany
[b] Institute for Materials in Energy Systems, Forschungszentrum Jülich, Germany

(Received 13 September 1993; accepted 9 November 1993)

Abstract

Crack propagation in three materials (two commercial, one laboratory) produced by directed metal oxidation in a SiC filler was investigated. Crack growth was studied in situ *with CT specimen in the scanning electron microscope. Crack tip shielding by the formation of elastic, frictional and ductile crack bridging elements could be observed. R-curve behaviour was found with increases in fracture toughness from about 4 MPa.m$^{1/2}$ to 7·5 MPa.m$^{1/2}$ over a crack length of about 1·5 mm. Near crack tip opening displacements provided an estimate of the crack tip toughness value, T_0 = 2·0 ± 0·6 MPa.m$^{1/2}$. COD measurements at the loadline allowed a distinction between large-scale and small-scale bridging regimes.*

Der Rißfortschritt in drei Werkstoffen, die durch gerichtete Schmelzoxidation in ein SiC Füllermaterial hergestellt wurden (davon zwei kommerzielle und ein Werkstoff aus dem eigenen Labor), wurde untersucht. Die Studien zur Rißausbreitung wurden in situ *in einem Rasterelektronenmikroskop an Kompaktproben durchgeführt. Dabei wurde Rißabschirmung durch Bildung von elastischen und duktilen Brücken, wie auch von Reibungsbrücken beobachtet. Die ermittelten R-Kurven zeigten einen Anstieg der Bruchzähigkeit von 4 MPa.m$^{1/2}$ auf 7·5 MPa.m$^{1/2}$ über eine Rißausdehnung von 1·5 mm. Die Messung der Rißöffnung nahe der Rißspitze erlaubt eine Abschätzung der Rißspitzenbruchzähigkeit, T_0 = 2·0 ± 0·6 MPa.m$^{1/2}$. Eine Unterscheidung zwischen großen und kleinen Brückenzonen wird durch die Messung der Rißöffnung an der Lastlinie ermöglicht.*

On a étudié la propagation des fissures dans trois matériaux (deux de qualité commerciale, l'un de laboratoire) produits par oxydation dirigée d'un métal au sein d'une matrice de SiC. On a observé la propagation in situ *au microscope à balayage dans des échantillons pour tests CT. On a pu examiner l'écrantage en pointe de fissure par la formation de ponts au niveau de cette fissure, de nature élastique, de friction, ou de nature ductile. On a déterminé la résistance à la propagation de fissures; la ténacité augmente, passant de 4 MPa.m$^{1/2}$ à 7·5 MPa.m$^{1/2}$ sur une longueur de fissure de 1·5 mm environ. On a obtenu une estimation de la ténacité en pointe de fissure: T_0 = 2·0 ± 0·6 MPA.m$^{1/2}$, en mesurant l'écartement près de la pointe. Enfin, la mesure de l'écartement le long de la ligne de chargement a permis de distinguer deux régimes de formation des ponts d'écrantage, l'un à petite échelle, l'autre à grande échelle.*

1 Introduction

Ductile phase toughening of brittle materials has received new interest over the last few years, both in the field of ceramics[1–5] as in the field of intermetallics[6–9]. The ensuing research centred on the realisation that crack bridging with attendant closure forces across the crack faces[10,11] can be utilised in a more general manner than process zone shielding[12] in order to toughen ceramics. Furthermore, the production of ceramic matrix materials via directed metal oxidation[13] allowed large-scale manufacture of ductile phase reinforced ceramics. Vital precedents of ductile phase toughening could be drawn on in the work on cemented carbides, stemming largely from research performed in the late 1970s,[14,15] but also late 1980s[16–18]. A second, seemingly independent, line came from an interest in ductile phase toughening in glasses,[19] where also crack bridging arguments were developed.[20]

* Present address: FG Nichtmet. Anorg. Werkstoffe, Hilpertstrasse 31, Building D, 64295 Darmstadt, Germany.

Journal of the European Ceramic Society 0955-2219/94/$7.00

It is now well appreciated that ceramic matrix composites reinforced by ductile phases can offer properties such as high hardness and wear resistance (based predominantly on the ceramic constituent), high fracture toughness, K_{Ic} (as in WC/Co with a value of 15 MPa.m$^{1/2}$),[16] high fracture, σ_f (as in Al/Al_2O_3 with a value of 760 MPa)[21] and high Weibull modulus, m (as in Zr/ZrB_2/ZrC with $m = 68$).[22]

There is general agreement that the toughening contribution by plastic deformation of the ductile phases is governed by the yield strength of the metal constituent and its uniaxial flow stress as established under the constraint of the more or less well bonded interface between metal and brittle matrix. The change of uniaxial stress, p, in the bridging ligament with crack opening, $2u$, is represented by a stress displacement function, $p(u)$, which uniquely describes the reinforcement characteristic[23] and in a different description leads to the increasing fracture resistance with crack extension $R(\Delta c)$.

Experimental efforts at this stage are mainly centered around either studies to determine the $p(u)$ function in model systems[3,6,7] or are restricted to post-fracture investigations of the final ductile phase elongation.[2] Very recently, however, actual R-curve measurements were reported. These were performed in three point bending on materials produced by directed metal oxidation,[24] in a model lead/glass composite[25] and via indentation fracture in a B_4C/Al composite.[26]

A final issue concerns the existence of plastic deformation in a process zone which might superimpose on the toughening effect due to crack bridging. A high-resolution strain mapping technique used to measure the plastic dissipation in the ductile phase in three cemented carbides provided strong evidence, that process zone as well as crack face mechanisms have to be considered to understand ductile phase toughening at least in this material category.[27]

While we are now in a position to semi-quantitatively reproduce the total energy dissipation of the ductile ligament up to rupture, we require more reliable data ($p(u)$, $R(\Delta c)$) to describe the complete evolution of constrained ductile phase stretching. These measurements should preferably be taken in standard fracture mechanics specimens which are well away from dangers of measuring large scale bridging artefacts, as might occur in three-point or four-point bending.[28,29] If a rising R-curve cannot be measured at small crack lengths, a measure of the crack tip toughness could provide at least the starting point of the crack resistance curve. We further require detailed observations of ductile phase deformation during loading and crack propagation to gain further insight into the crack/reinforcement interactions in these types of composites. Three different metal–ceramic composites produced by directed metal infiltration into a SiC filler material were therefore chosen in order to measure the R-curve in CT specimen, as well as the crack tip toughness, T_0, in these materials and to correlate the measurements with in situ crack propagation observations in the SEM.

2 Experimental

Two commercial Al/SiC/Al_2O_3 materials (Alanx FGS (Material FGS) and Alanx CG273 (Material CGS), Alanx Products L. P., Newark, DE, USA) and one composite prepared at TUHH[30] were chosen for mechanical property characterisation. The commercial grade is described as (i) FGS (fine grain size) composite with a SiC content of 68·7%, a maximum SiC grain size of 65 μm and an elastic modulus E of 366 GPa and (ii) CGS (coarse grain size) composite with a SiC content of 86·6%, a maximum SiC grain size of 220 μm and an elastic modulus of 313 GPa. The high SiC-loading in the CGS material is explained by a bimodal SiC particle size distribution with small particles filling the gaps between the large particles. The material prepared in the own laboratory (FGSL) had a SiC content of 51%, a maximum SiC grain size of 100 μm and an elastic modulus of 350 GPa.

Figure 1 provides an optical micrograph of the microstructure of the CGS composite with SiC shown as large particles distributed through a matrix consisting of the alumina grains (dark) and metal phase (white). The metal phase contains about 15% silicon. The silicon has to be added to ensure thermodynamic stability for the SiC grains at the processing temperature of 1050–1100°C.[30]

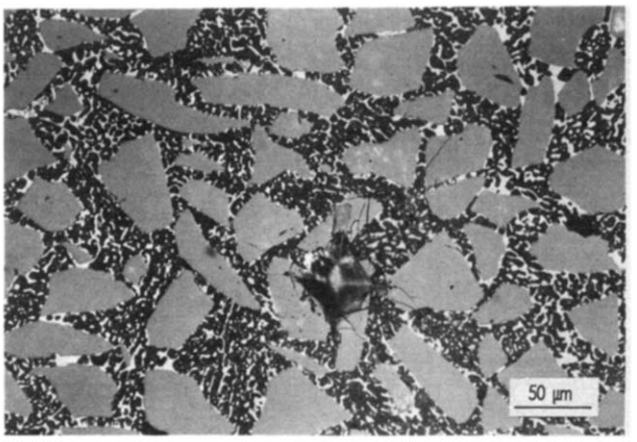

Fig. 1. Optical micrograph providing overview of microstructure of CGS composite. Residual contact zone of Vickers indentation leaves ill-defined crack pattern.

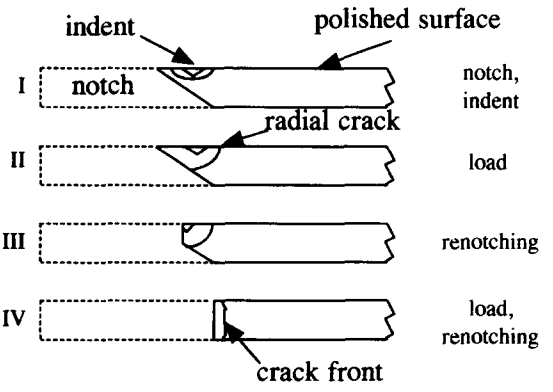

Fig. 2. Schematic illustrates procedure to generate through-thickness precrack in CT specimen.

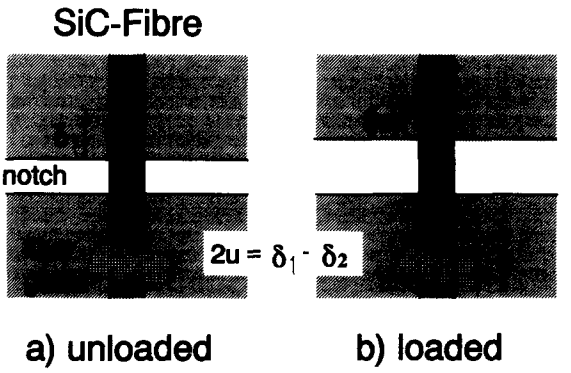

Fig. 3. Schematic outlines measurement of differential displacement across notch between (a) unloaded, and (b) loaded state using a SiC fibre as measurement flag.

Radial cracks from Vickers indentations do not provide a well described crack pattern in these types of composites (optical micrograph: Fig. 1). For this reason, CT specimens were chosen for crack propagation studies, R-curve measurements and determination of the crack opening displacement (COD). Notch lengths between 4 and 6 mm were used. CT specimens were machined according to instructions in ASTM E-399,[31] but with a thickness, t, of 1·5 mm. The distance from load-line to edge of the specimen, w, was either 18 or 20 mm. S-DCB specimen[32] were also produced from the FGSL composite and investigated separately.

Qualitative and quantitative crack propagation studies of the commercial materials were performed in situ in the scanning electron microscope with a self-designed device for loading CT specimen.[23,33] The device allows direct observation of bridge (any microstructural element providing a closure force) evolution, measurement of applied load and crack tip position, which, in combination allows computation of the R-curve, but also measurement of the crack opening displacement profile. The FGSL composite was tested in a commercial load frame with the crack tip being monitored with a travelling microscope using oblique illumination.

Controlled and reproducible crack initiation remains a constant source of trouble for fracture propagation studies in ceramics. Our procedure for precracking CT specimen, based on a mechanism described in an earlier report,[23] is therefore described here in detail in Fig. 2. (1) A half-chevron notch was sawn to extend the original notch. The upper polished side was then indented with an indentation load of 49 N at a distance of about 200 μm to the notch tip. (2) The specimen was then loaded in the *in situ* fracture device, which was situated on the stage of an optical microscope. (3) After crack extension of about 300 μm the (straight) notch is extended. This eliminates part of the active crack bridges and reduces the necessary load for further crack extension, putting crack extension back into the steep part of the R-curve and thereby into the stable crack propagation regime. (4) Loading and subsequent renotching is continued until the crack has propagated into the constant thickness regime of the specimen.

The crack opening displacement at the notch was measured as described in Fig. 3. A SiC fibre was glued down on one side of the notch and the position of superficial marks of the fibre with respect to characteristic microstructural features or the notch edge determined in the unloaded state. This distance was measured in the loaded state, and the differential taken as the crack opening displacement in the notched area. This procedure typically was followed at the load line and at an additional position about half-way between load line and notch tip.

3 Results

3.1 Qualitative observations

Crack propagation in the Al/SiC/Al_2O_3 was found to be discontinuous with crack jumps between 10 and 80 μm and in one instance of up to 1 mm just before final instability in the FGS material. Crack propagation could be studied over lengths of 0·5–1·5 mm in the coarse grained SiC composite and over 1·7 mm in the fine grained SiC composite. Secondary cracks were rarely, microcracks not observed.

A general overview of the FGS material including a crack tip regime is provided in a SEM micrograph in Fig. 4. The gray areas represent the SiC grains, the dark areas the ductile phase while the bright areas show the alumina grains. Crack propagation frequently occurs along Al/SiC (A) and SiC/Al_2O_3 (B) interfaces. This occasionally leads to the formation of frictional bridges as depicted in Fig. 5, where a large SiC grain is seen being pulled out of its socket. Intact, elastic

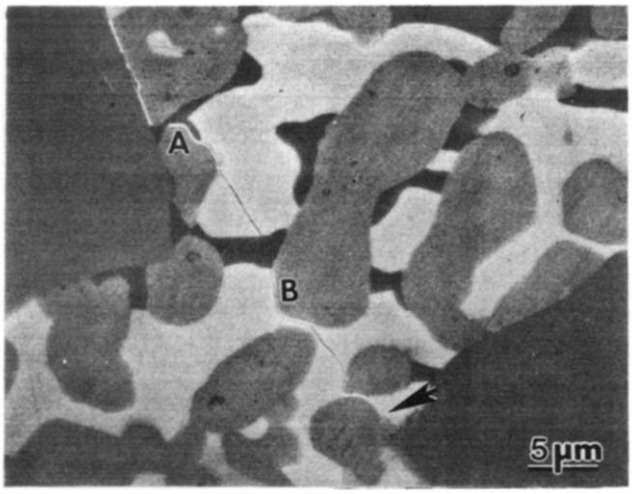

Fig. 4. SEM micrograph shows representative crack path through FGS composite including crack tip as marked by arrow. 'A' and 'B' mark sites of crack propagation along Al/SiC and SiC/Al_2O_3 interfaces, respectively. Cracks are always shown propagating from top to bottom.

bridges as shown in Fig. 6, appear to occur somewhat more frequently than the aforementioned frictional bridges. Elastic bridges can occur in various size regimes. An evolution of a set of elastic microbridges is provided in Fig. 7. These types of reinforcing elements are related to transgranular fracture. The example given in Fig. 7 shows a 'right-stepping crack' as it advances through a SiC grain of about 20 μm diameter. Step-by-step evolution of these bridge formations could not be resolved. The local bridge formation, once formed, remained unchanged during further crack propagation, except for ligament fracture as shown in Fig. 7(b). Local crack tip positions of elastic bridges therefore remained constant and the local compliance of these reinforcing elements remained unchanged. Bridging elements remained effective up to large CODs of up to 0·5 μm (as can be seen in Fig. 7(a)).

The evolution of ductile reinforcements is given

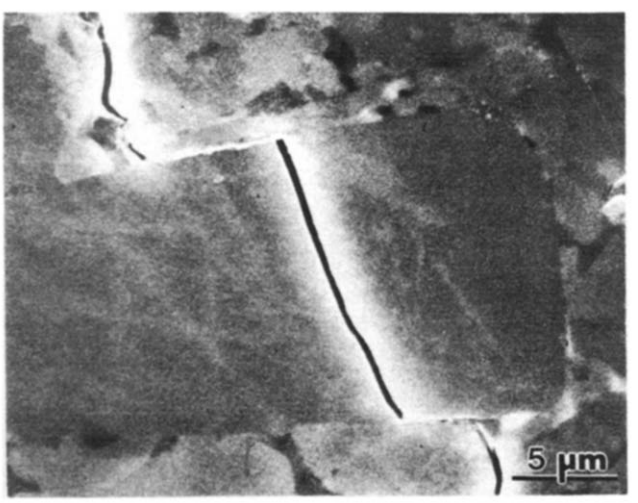

Fig. 5. Crack deflection at SiC grain/matrix interface gives rise to the formation of frictional bridge at SiC grain in FGS composite.

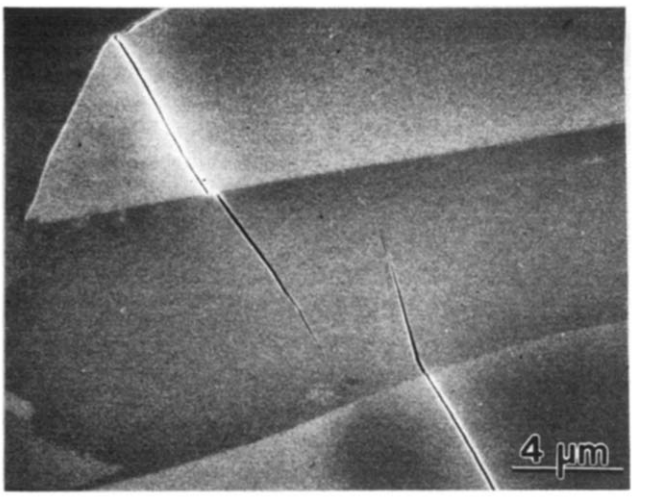

Fig. 6. Large elastic bridge in FGS composite is viewed in SiC grain in region 350 μm from the crack tip.

in Figs 8 and 9. Occasionally, the crack branches before the metal ligament. Crack blunting can be observed at the first crack–ligament contact point. From surface observations no interface debonding could be found. Ligament failure was governed by hole nucleation and hole growth in the ductile phase. Again, the detailed evolution of the plastic deformation of the reinforcement could not be followed. These bridging elements were effective up to CODs of more than 0·5 μm.

Correlation can be sought between bridge evo-

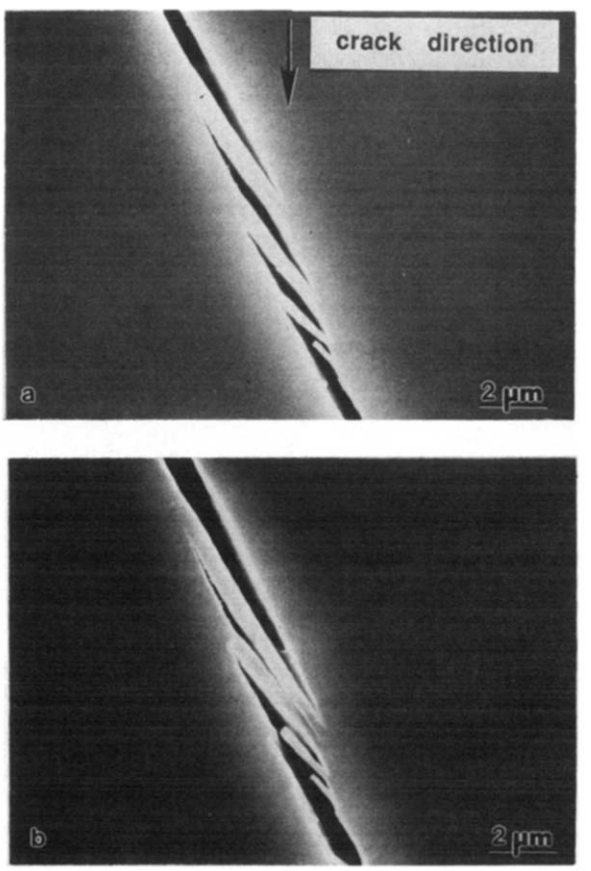

Fig. 7. Evolution of elastic bridges in CGS composite formed by intergranular fracture of large SiC grain at position (a) 410 μm, and (b) 530 μm from crack tip.

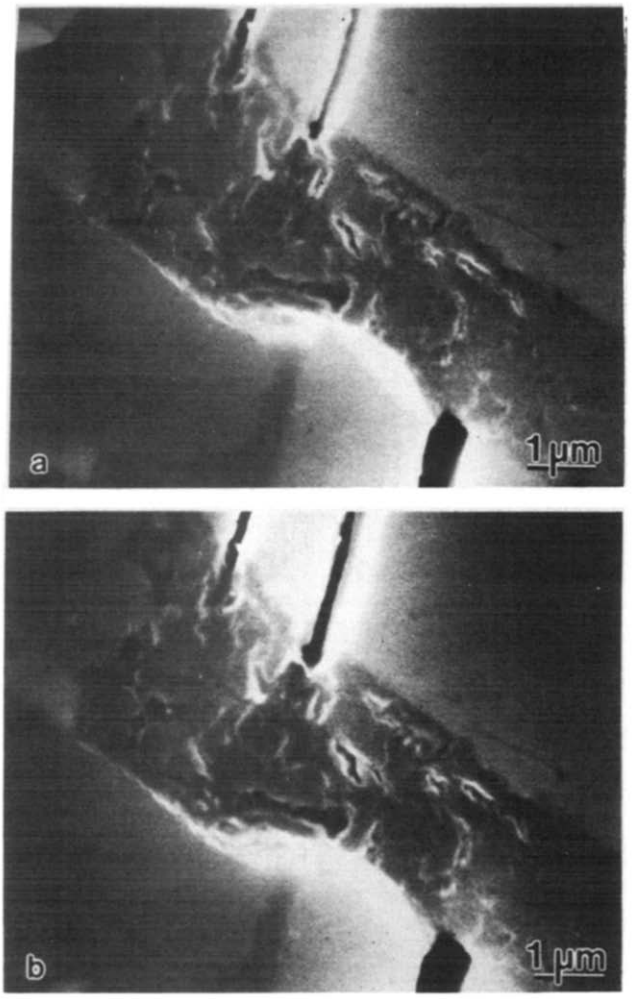

Fig. 8. SEM micrographs provide sequence for metal ligament deformation, which is situated (a) 360 μm, and (b) 400 μm behind the crack tip (FGS composite).

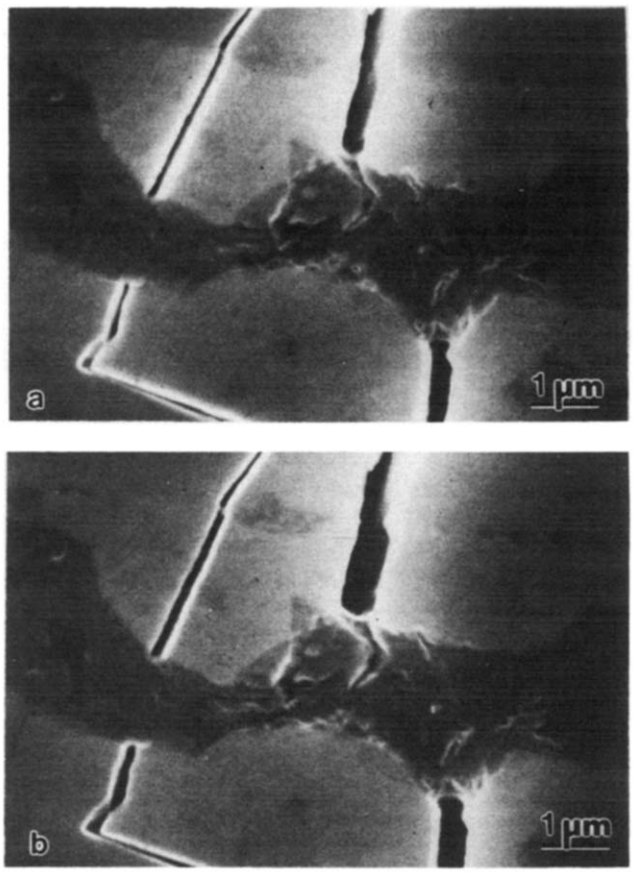

Fig. 9. Similar sequence to Fig. 8 shows response of metal ligament to increasing local crack opening with distance to the crack tip (a) 300 μm, and (b) 340 μm (FGS composite).

lution from *in situ* crack propagation studies of the specimen surface to post-fracture investigations at the crack faces. A representative example for a very tortuous fracture in the SiC grains, which might represent stepwise cleavage fracture, is provided in Fig. 10. Fracture surfaces as shown here are a necessary but not a sufficient requirement to provide elastic bridging elements as detailed in Fig. 7. Figure 11 gives an illustration for ductile fracture occurring at Al/SiC interfaces. Strong bonding between aluminium and silicon carbide leads to plastic dissipation for crack propagation along this particular interface. Examples for only limited debonding at Al/SiC interfaces are also provided in Figs 12(a) and (b). Ligament failure through hole nucleation and hole growth is also demonstrated in this figure where several dimples are seen to have formed at the metal fracture surface.

3.2 R-curve measurements

Starter cracks in the CT specimen were already longer than 200 μm. The fracture toughness in the FGS material increased (Fig. 13) from 3·9 MPa.m$^{1/2}$ at a bridged crack length Δc of 260 μm to 6 MPa.m$^{1/2}$at Δc of 560 μm and further to 7·5 MPa.m$^{1/2}$ at Δc = 1730 μm. Materials with high volume fraction of coarse grained SiC (CGS) showed only moderate R-curve behaviour. Specimen CGS(A) showed an increase in fracture toughness from 4·3 MPa.m$^{1/2}$ to 5·1 MPa.m$^{1/2}$ during crack growth from Δc = 360 μm to Δc = 460 μm. A similar increase in fracture toughness (from 3·8 MPa.m$^{1/2}$ to 4·9 MPa.m$^{1/2}$) was found in specimen CGS(B) during crack growth from Δc = 540 μm to Δc = 1540 μm.

R-curves from the FGSL material are not avail-

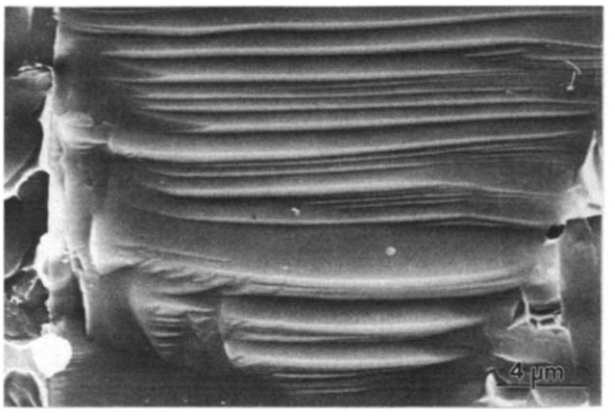

Fig. 10. Example for stepwise cleavage fracture provides hint for possible existence of elastic bridges (FGS composite).

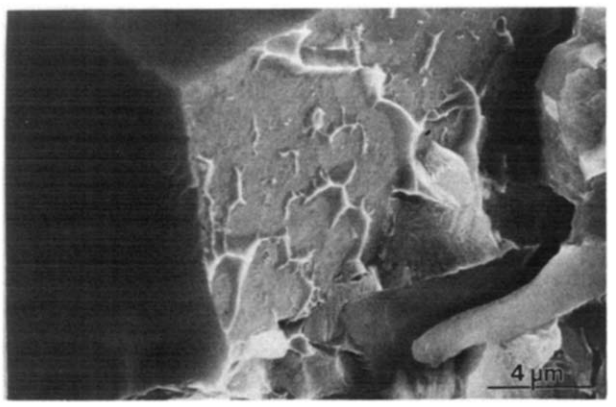

Fig. 11. Fracture surface shows ductile deformation for the case where the crack propagated along SiC/metal interface (FGS composite).

able since the specimen broke in transition from the half-chevron regime into the constant thickness region. At this instability point a single fracture toughness value of 6·7 MPa.m$^{1/2}$ with a bridged crack length of 4·88 mm can be provided. The bridged crack length appears sufficient to provide a plateau value on the R-curve. One might note, though, that the bridging zone was not in the constant thickness area, therefore only a friction of possible bridging sites is activated. The actual steady state toughness of this material is

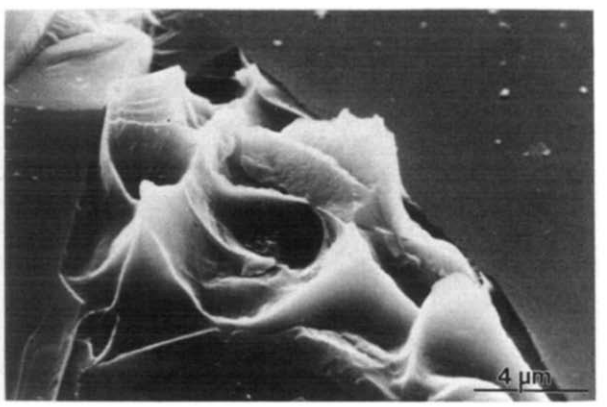

(a)

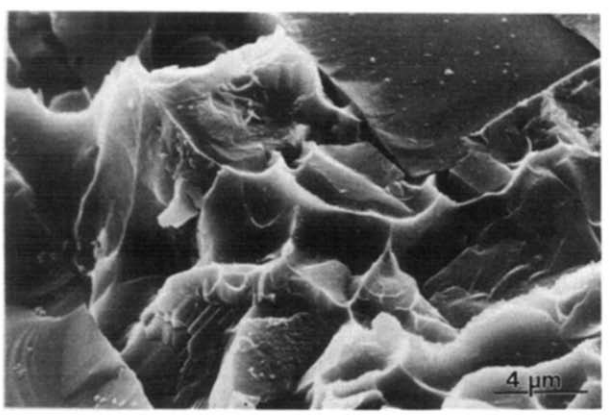

(b)

Fig. 12. Examples of fracture surfaces, (a) and (b), show limited degree of debonding between metal and SiC grain with failure of metal ligament through cavitation (FGS composite).

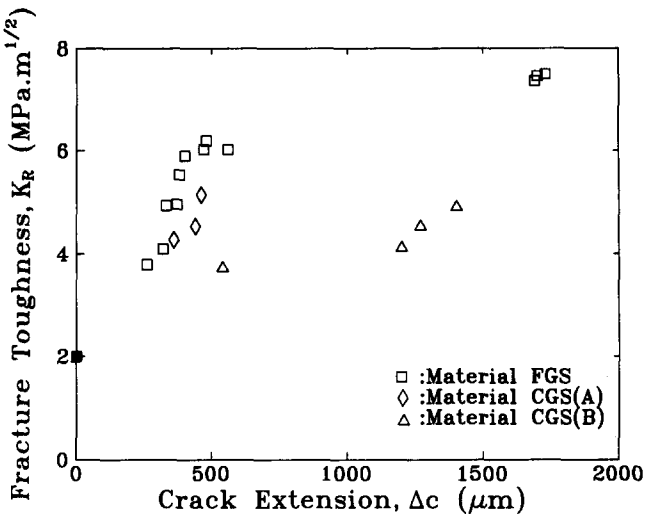

Fig. 13. R-curves for FGS composite specimen and two CGS specimens. The fracture toughness value at $\Delta c = 0$ stems from a determination of the crack tip toughness (see COD measurements and discussion).

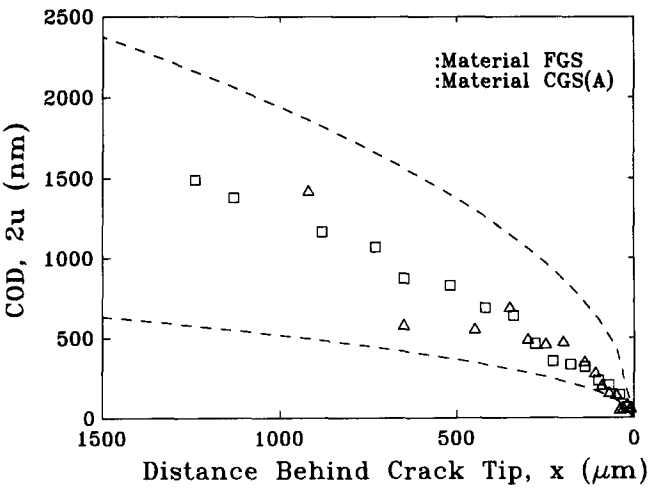

(a)

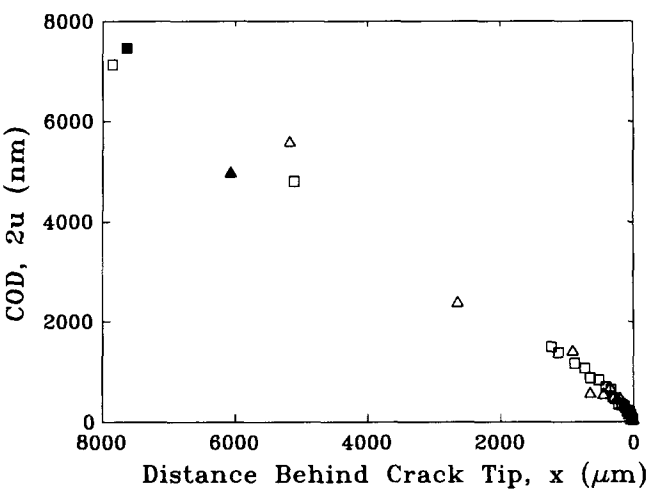

(b)

Fig. 14. (a) Crack opening displacement as function of the distance from the crack tip for FGS as well as CGS composite. Dashed lines are inner parabola for T_0 = 2·0 MPa.m$^{1/2}$ and outer parabola for K_A = 7·0 MPa.m$^{1/2}$ for FGS composite. (b) Crack opening displacement as measured as distance between crack surfaces and as determined by differential displacement of measurement flag at notch. Also included (filled symbols) are predictions for loadline displacements according to eqn (2).

therefore expected to lie somewhat higher than the value given above.

3.3 COD measurements

Crack opening displacements for one specimen each of material FGS (at K_A = 7·0 MPa.m$^{1/2}$) and CGS (at K_A = 4·5 MPa.m$^{1/2}$) are provided in Fig. 14. In the limit of long cracks in large specimen COD data near the crack tip generally lie in a coordinate space confined by an inner and outer parabola which are both described by the Barenblatt[34] relation for stress-free crack surfaces (eqn 1):

$$u(x) = \sqrt{\frac{8x}{\pi}} \frac{K_A}{E'} \tag{1}$$

with u being half the crack opening, x the distance from the crack tip, K_A the applied stress intensity factor and E' the plane strain Young's modulus. The inner and outer parabolas for Fig. 14(a) were plotted for the material FGS with K_A = 2·0 MPa.m$^{1/2}$, and 7·0 MPa.m$^{1/2}$, respectively. The first fracture toughness value corresponds to the crack tip toughness of this material (see discussion), the latter value to the applied stress intensity factor at the moment the measurement was taken (the corresponding value for the CGS material was 4·5 MPa.m$^{1/2}$).

Figure 14(b) reproduces the COD data on the scale of the total crack length c, including the notch back to the loadline. Crack opening displacement values gained by applying the technique described in Fig. 3 are now also folded into the graph. In addition, theoretically predicted CODs at the loadline ($2u_l$), based on the crack–specimen geometry (c,w,t) and the applied load P are also provided in form of full symbols. These are determined based on a handbook solution[35] (eqn 2):

$$2u_l = \frac{P}{tE'} v_2(c/w) \tag{2}$$

with eqn (3):

$$v_2(c/w) = \frac{\frac{c}{w}}{\left(1-\frac{c}{w}\right)^2}\left(38{\cdot}2 - 55{\cdot}4\frac{c}{w} + 33{\cdot}0\left(\frac{c}{w}\right)^2\right) \tag{3}$$

4 Discussion

In situ crack propagation studies allow observation of frictional bridges and particularly of elastic bridges aside from the expected ductile bridging elements. Fracture surfaces repeatedly exhibit stepwise cleavage fracture and point to possible elastic bridging sites. Metal ligaments fail through multiple cavity nucleation and cavity growth, with good correlation between crack propagation studies on the surface and fracture surface observations. The occurrence of plastic dissipation during crack propagation along SiC/Al interfaces and a limited degree of debonding during plastic stretching of the metal ligaments points to the existence of a 'strong' interface between SiC and Al. Limited debonding then leads to the formation of high hydrostatic stresses in the metal ligament, which mediates hole nucleation as only possible deformation mechanism. It is, however, unclear to what degree the existence of silicon precipitates in the metal contributed to hole formation. Contrary to the study by Flinn *et al.*,[2] where precipitates could be found in the bottom of some of the holes, no correlation between precipitate distribution and nucleation site could be obtained. Also, multiple hole nucleation, rather than single hole formation in the centre of the ligament[2] appeared to define final ligament failure.

The complexity of this real system disallows definite modelling beyond a computation of 'ballpark numbers' to separate and to attach a definite percentage of toughness increment to each brittle reinforcement type as compared to the ductile reinforcements. Both types of bridging elements provide definite bridging stresses which, with increasing crack length, can be integrated with the appropriate weighing factor to account for the observed R-curve behaviour.

A rising crack resistance curve can be measured which, if knowledge about the crack tip toughness value of 2 MPa.m$^{1/2}$ is included, spans a region from 2 to 6 MPa.m$^{1/2}$ in the FGS material and from 2 to 5 MPa.m$^{1/2}$ in the CGS material, both in the first 500 μm of crack extension. The FGS composite had a higher metal content which appeared responsible for a steeper R-curve and accompanying smaller crack jumps and higher fracture toughness than the CGS composite. The latter had a bimodal size distribution of the SiC filler with grain sizes up to 220 μm which is suggested to be responsible for large inhomogeneities on the microstructural scale and therefore for the differing R-curves for the two samples measured.

The use of CT specimens for measuring R-curve behaviour in metal reinforced ceramics is preferred to using three-point bend specimens[24,28,29] where artefacts due to large-scale bridging frequently occur.[28,29] The total increase in fracture toughness in our study (3–5·5 MPa.m$^{1/2}$) can, however, be compared to data obtained on comparable DMO composites[24] which typically were found to be in the order of 2 MPa.m$^{1/2}$. The relatively large increase in fracture toughness in our investigations is partly due to the inclusion of the crack tip fracture toughness value.

The procedure to obtain the value for the crack tip toughness, T_0, relies on a measurement of the near crack tip opening displacement. The uncertainty in the determination of the crack opening displacement carries an uncertainty of about 0·5 MPa.m$^{1/2}$. A further, though small uncertainty, derives from the necessity to take the measurement at a finite distance from the crack tip. In the regime close to the crack tip the COD can be approximated by the general Barenblatt profile,[34] which, in this case, includes closure stresses at the crack faces:

$$u(x) = \sqrt{\frac{8x}{\pi}}\frac{T_0}{E'} + \frac{4}{\pi E'}\int_0^{c_b} p(x') \times \left(\sqrt{\frac{x}{x'}} - \frac{1}{2}\ln\left(\left|\frac{\sqrt{x'}+\sqrt{x}}{\sqrt{x'}-\sqrt{x}}\right|\right)\right) dx' \quad (4)$$

Here, E' is the plane strain Young's modulus, x a field point where $u(x)$ is computed and x' a source point where closure stresses are active. Solving for the crack tip toughness T_0 yields:

$$T_0 = u(x)E'\sqrt{\frac{\pi}{8x}} - \sqrt{\frac{2}{\pi x}}\int_0^{c_b} p(x') \times \left(\sqrt{\frac{x}{x'}} - \frac{1}{2}\ln\left(\left|\frac{\sqrt{x'}+\sqrt{x}}{\sqrt{x'}-\sqrt{x}}\right|\right)\right) dx' \quad (5)$$

The integral term vanishes at the crack tip, but still gives a minor contribution to T_0 at small x (typically 10–30 μm from the crack tip), where the COD measurements for determining T_0 are taken. An upper bound for the integral term can be found by substituting $p(x')$ through an upper estimate of the maximum closure stress close to the crack tip. Analytical integration[36] then gives the correction term due to the finite distance to the crack tip. This measurement inaccuracy was found to be smaller than 0·1 MPa.m$^{1/2}$ for the case of an arbitrarily chosen, but high maximum closure stress P_m = 300 MPa.

A crack tip toughness value, T_0 of 2·0 ± 0·6 MPa.m$^{1/2}$ for our composites was found and can be compared with values of T_0 = 2·0 MPa.m$^{1/2}$ for alumina[23] and to values of T_0 = 2·5 MPa.m$^{1/2}$ for a SiC whisker reinforced alumina.[37] Though specific details and differences of grain boundary chemistry between these three materials will have some effect on the crack tip toughness, these values nevertheless provide some indication that the aluminium metal inclusions do not affect the crack tip toughness to a large degree, but lead to crack wake effects only. One might also point out that a possible toughening effect due to a plastic stretch process zone is not expected to occur in composites containing metals with low yield strength[38] (as in aluminium with about 50 MPa). This is to be seen in contrast to for example, WC/Co composites where metal yield strengths in excess of 2 GPa (Ref. 18) may be responsible for an appreciable contribution of a process zone[27] to a fracture toughness increment besides crack bridging.

A direct measure of the COD at the loadline allows comparison with calculated values which are based on the size of specimen and unbridged cracks. This measure can therefore give an indication whether small scale bridging or large scale bridging is in effect. In the first case the closure stresses close to the crack tip will not affect the COD at the loadline and computed and measured data will coincide (our case). In the latter case the measured COD should lie well below the calculated value, since closure stresses have not been relaxed over the relatively small distance between bridging site and loadline.

6 Conclusions

The following conclusions are made.

(1) *In situ* crack propagation studies on various materials produced by directed metal oxidation provide evidence for elastic SiC grain bridging, frictional SiC grain bridging and ductile ligament bridging, with the latter failing by multiple cavity nucleation and cavity growth.

(3) R-curves using a crack instability criteria from 3·9 to 7·5 MPa.m$^{1/2}$ and from 3·8 to 5·1 MPa.m$^{1/2}$ could be obtained in the DMO composites.

(3) The crack tip toughness in these materials was found to be 2·0 MPa.m$^{1/2}$.

Acknowledgements

This work was supported by the Volkswagen Foundation under contract number I/66 790.

References

1. Sigl, L. S., Mataga, P. A., Dalgleish, B. J., McMeeking, R. M. & Evans, A. G., On the toughness of brittle materials reinforced with a ductile phase. *Acta Metall.*, **36** (1988) 945–53.
2. Flinn, B. D., Rühle, M. & Evans, A. G., Toughening in composites reinforced with Al. *Acta Metall.*, **37** (1989) 3001–6.
3. Ashby, M. F., Blunt, F. J. & Bannister, M., Flow characteristics of highly constrained metal wires. *Acta Metall.*, **37** (1989) 1847–57.
4. Mataga, P. A., Deformation of crack-bridging ductile reinforcements in toughened brittle materials. *Acta Metall.*, **37** (1989) 3349–59.
5. Bao, G., & Hui, C.-Y., Effects of interface debonding on the toughness of ductile-particle reinforced ceramics. *Int. J. Sol. Struct.*, **26** (1990) 631–42.

6. Cao, H. C., Dalgleish, B. J., Deve, H. E., Elliott, C., Evans, A. G., Mehrabian, R. & Odette, G. R., A test procedure for characterizing the toughening of brittle inter-metallics by ductile reinforcements. *Acta Metall.*, **37** (1989) 2969–77.
7. Deve, H. E., Evans, A. G., Odette, G. R., Mehrabian, R., Emiliani, M. L. & Hecht, R. J., Ductile reinforcement toughening of γ-TiAl: effects of debonding and ductility. *Acta Metall.*, **38** (1990) 1491–502.
8. Lu, T. C., Evans, A. G., Hecht, R. J. & Mehrabian, R., Toughening of $MoSi_2$ with a ductile (niobium) reinforcement. *Acta Metall. Mater.*, **39** (1991) 1853–62.
9. Xiao, L. & Abbaschian, R., Interfacial modification in $Nb/MoSi_2$ composites and its effects on fracture toughness. *Mater. Sci. Engng*, **A155** (1992) 135–45.
10. Knehans, R. & Steinbrech, R. W., Memory effect of crack resistance during slow crack growth in notched Al_2O_3 bend specimens. *J. Mater. Sci. Lett.*, **1** (1982) 327–9.
11. Swanson, P. L., Fairbanks, C. J., Lawn, B. R., Mai, Y.-W. & Hockey, B. J., Crack interface grain bridging as a fracture resistance mechanism in ceramics: experimental study on alumina. *J. Am. Ceram. Soc.*, **70** (1987) 279–89.
12. Evans, A. G. & Cannon, R. M., Toughening of brittle solids by martensitic transformations. *Acta Metall.*, **34** (1986) 761–800.
13. Newkirk, M. S., Urquhart, A. W., Zwicker, H. R. & Breval, E., Formation of Lanxide™ ceramic composite materials. *J. Mater. Res.*, **1** (1986) 81–9.
14. Evans, A. G., Heuer, A. H. & Porter, D. L., Toughening mechanisms in cemented carbides. In *Proc. 4th. Int. Conf. Fracture*, ed. D. M. R. Taplin. Pergamon Press, New York, USA, 1977, pp. 529–56.
15. Nakamura, M. & Gurland, J., The fracture toughness of WC-Co two-phase alloys—a preliminary model. *Metall. Trans.*, **11A** (1980) 141–6.
16. Sigl, L. S., Das Zähigkeitsverhalten von WC–Co–Legierungen. *Fortschrittberichte VDI*, **5**(104) (1986).
17. Sigl, L. S. & Exner, H. E., Experimental study of the mechanics of fracture in WC–Co alloys. *Metall. Trans.*, **18A** (1987) 1299–308.
18. Sigl, L. S. & Fischmeister, H. F., On the fracture toughness of cemented carbides. *Acta Metall.*, **36** (1988) 887–97.
19. Krstic, V. V., Nicholson, P. S. & Hoagland, R. G., Toughening of glasses by metallic particles. *J. Am. Ceram. Soc.*, **64** (1981) 499–504.
20. Krstic, V. V., On the fracture of brittle-matrix/ductile-particle composites. *Philos. Mag.*, **A48** (1983) 695–708.
21. Wu, S., Gesing, A. J., Travitzky, N. A. & Claussen, N., Fabrication and properties of Al-infiltrated RBAO-based composites. *J. Eur. Ceram. Soc.*, **7** (1991) 277–81.
22. Claar, T. D., Johnson, W. B., Anderson, C. A. & Schiroky, G. H., Microstructure and properties of platelet-reinforced ceramics formed by the directed reaction of zirconium with boron carbide. *Ceram. Engng Sci. Proc.*, **10** (1989) 599–609.
23. Rödel, J., Kelly, J. F. & Lawn, B. R., In situ measurements of bridged crack interfaces in the scanning electron microscope. *J. Am. Ceram. Soc.*, **73** (1990) 3313–18.
24. Pickard, S. M., Manor, E., Ni, H., Evans, A. G. & Mehrabian, R., The mechanical properties of ceramic composites produced by melt oxidation. *Acta Metall. Mater.*, **40** (1992) 177–84.
25. Bannister, M., Shercliff, H., Bao, G., Zok, F. & Ashby, M. F., Toughening in brittle systems by ductile bridging ligaments. *Acta Metall. Mater.*, **40** (1992) 1531–7.
26. Bhattacharya, A. K. & Petrovic, J. J., Ductile phase toughening and R-curve behaviour in a B_4C—Al cermet. *J. Mater. Sci.*, **27** (1992) 2205–10.
27. Marshall, D. B., Morris, W. L., Cox, B. N. & Dadkhah, M. S., Toughening mechanisms in cemented carbides. *J. Am. Ceram. Soc.*, **73** (1990) 2938–43.
28. Zok, F. & Hom, C. L., Large scale bridging in brittle matrix composites. *Acta Metall. Mater.*, **38** (1990) 1895–904.
29. Flinn, B. D., Lo, C. S., Zok, F. W. & Evans, A. G., Fracture resistance of a metal-toughened ceramic. *J. Am. Ceram. Soc.*, **76** (1993) 369–75.
30. Sindel, M. PhD thesis, TUHH, Germany, 1993.
31. ASTM, *Annual Book of ASTM Standards* (Vol. 3.01, E-399-83). American Society for Testing and Materials, Philadelphia, PA, USA, 1989, pp. 480–504.
32. Heuer, A. H., Readey, M. J. & Steinbrech, R. W., Resistance curve behavior of supertough MgO–partially-stabilized ZrO_2. *Mater. Sci. Engng.*, **A105/106** (1988) 83–9.
33. Rödel, J., Kelly, J. F., Stoudt, M. R. & Bennison, S. J., A loading device for fracture testing of compact tension specimen in the SEM. *Scanning Electron Microscopy*, **5** (1991) 29–35.
34. Barenblatt, G. I., The mathematical theory of equilibrium cracks in brittle fracture. *Adv. Appl. Mechan.*, **7** (1962) 55–129.
35. Tada, H., Paris, P. C. & Irwin, G. R., *The Stress Analysis Handbook*. Paris Productions, St Louis MO, USA, 1985.
36. Rödel, J., Interaction between crack bridging and crack deflection. *J. Eur. Ceram. Soc.*, **10** (1992) 143–50.
37. Rödel, J., Fuller Jr., E. R. & Lawn, B. R., In situ observations of toughening processes in alumina reinforced with silicon carbide whiskers. *J. Am. Ceram. Soc.*, **74** (1991) 3154–7.
38. Tvergaard, V. & Hutchinson, J. W., The relation between crack growth resistance and fracture process parameters in elastic–plastic solids. *J. Mech. Phys. Solids*, **40** (1992) 1377–97.